Inflection points in the conduction-band structure of $BaSnO_3$

A. J. E. Rowberg, K. Krishnaswamy, and C. G. Van de Walle*
Materials Department, University of California, Santa Barbara, California 93106, USA

(Received 13 July 2020; accepted 24 August 2020; published 8 September 2020)

$BaSnO_3$ (BSO) is a wide-band-gap oxide in which very high levels of *n*-type doping have been demonstrated. Here we perform a detailed investigation of the conduction-band structure of BSO, reporting band velocities and effective masses as a function of energy, and explore whether sufficiently high doping levels can be achieved to fill the conduction band to energies near the inflection point. The presence of carriers near the inflection point can lead to negative differential resistance (NDR) due to the effective mass above the inflection point being negative. Our first-principles calculations, based on density functional theory with a hybrid functional, show that BSO has an inflection point 2.29 eV above the conduction-band minimum and that secondary conduction-band valleys are at least 2 eV higher in energy. We discuss the options available to achieve the required *n*-type doping levels to reach the inflection point in BSO.

DOI: 10.1103/PhysRevB.102.115201

I. INTRODUCTION

The dispersion of the conduction band (CB) plays an important role in the properties of semiconductors. The curvature of the CB determines the electron effective mass, which in turn determines electron mobility. High electron mobility is a distinguishing feature of $BaSnO_3$ (BSO), a perovskite stannate with a wide band gap that is being actively explored as a transparent conductor and also for power electronic devices such as high-frequency transistors [1]. A peak electron mobility of 320 $cm^2\ V^{-1}\ s^{-1}$ at 300 K has been observed in bulk BSO [2], the highest reported room-temperature mobility among perovskite oxides [3]. Thin films [4] and nanomembranes [5] of BSO have also demonstrated high mobility. The low electron effective mass [6,7] is associated with the high dispersion of the CB, which can be attributed to its Sn-*s* character [8]. The CB is not parabolic, however, which means that the effective mass changes as a function of the Fermi level (E_F), and, ergo, doping levels.

While mobility is associated with low-field transport, high-field transport depends on properties of the conduction band at higher energies. Nonparabolicity can lead to the presence of inflection points, as shown in Fig. 1. Above an inflection point, the electron effective mass becomes negative [9–11], which can give rise to a negative differential resistance (NDR) that can be exploited in oscillators. The band velocity initially increases with the applied electric field to reach a maximum and then decreases with a further increase in the field. NDR can also be caused by scattering to satellite valleys with heavier effective masses, giving rise to the Gunn effect, which can produce radiation up to 100 GHz [12,13]. NDR caused by the presence of an inflection point, on the other hand, does not require intervalley scattering and can lead to radiation at frequencies on the order of THz [9,14].

In this work, we present a detailed first-principles study of the CB structure of BSO up to energies more than 5 eV above the CB minimum (CBM). We report on the presence of inflection points and find that satellite valleys occur at energies at least 2 eV above the inflection points. We explore the effect of alloying on the position of inflection points. We also provide values of effective masses and band velocities as a function of energy in the CB. In addition, we explore whether electrons may be placed near the inflection point in BSO not by injection at high energies but by doping. Experimentally, electron concentrations up to $2 \times 10^{21}\ cm^{-3}$ in La-doped BSO have been reported [15].

Carriers can be introduced into BSO in several ways. In a heterostructure, electrons can be induced via modulation doping or polar discontinuity doping [16,17]. Encouraging results have been reported for interfaces with $(Sr,Ba)SnO_3$ [18], La-doped $SrSnO_3$ [19], $LaScO_3$ [20], and $LaInO_3$ [21]. However, the achievable electron concentrations will in such cases be limited by the CB offsets [17,22,23]. Electrons can also be introduced using donor doping, with lanthanum being the dopant that has most commonly and successfully been used for *n*-type doping of BSO [4,24,25]. First-principles calculations based on density functional theory (DFT) have also shown La to be an effective *n*-type dopant [26–28]. In particular, Ref. [27] showed that, under Sn-rich and O-poor synthesis conditions, electron concentrations resulting from La doping can surpass $10^{21}\ cm^{-3}$. We note that, as a wide-band-gap semiconductor, BSO can sustain high electric fields that, in combination with high doping levels, could assist in moving carriers to the negative-effective-mass regions of the Brillouin zone.

However, assessing whether a donor dopant is still effective at extremely high doping levels, where the CB is filled to a high E_F, requires further examination. Donor dopants have more valence electrons than the atom they replace in the lattice; in the case at hand, La (valence 3) substitutes on a Ba (valence 2) site. For a shallow donor, the extra

*Corresponding author: vandewalle@mrl.ucsb.edu

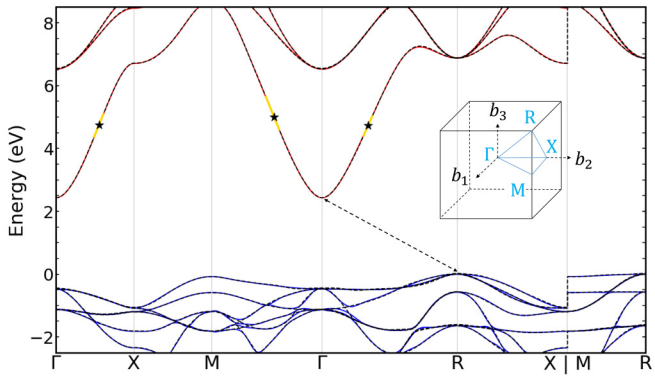

FIG. 1. Calculated band structure of $BaSnO_3$, comparing HSE results (solid lines) with Wannier interpolation (dashed lines). The lowest CB inflection points are indicated by stars. The yellow regions around the stars reflect portions of the band structure in which the slope varies by no more than 1% relative to the inflection points. Inset in the plot is a schematic of the Brillouin zone.

electron associated with this higher valence resides in an electronic state that is well above the CBM; i.e., it forms a resonance in the CB, as schematically indicated in Fig. 2(a). If one attempts a calculation for the neutral charge state of the donor, the electron contributed by the impurity will not reside in this impurity-induced state, but will transfer to the CB. The Coulomb attraction between this electron and the positively charged impurity center leads to the formation of a hydrogenlike state, which is typically described in hydrogenic effective-mass theory. In the vast majority of cases, one therefore pays scant attention to the actual impurity-induced state high in the CB, since its only function is to supply the electron. However, if the focus is on achieving high electron concentrations that will fill the CB to high levels of E_F, it needs to be verified that the impurity-related level is indeed high enough to continue donating electrons to the CB. If E_F rises above this level, the impurity will no longer function as a donor, and the electron will remain localized on the impurity.

II. COMPUTATIONAL METHODS

In our investigation, we conduct first-principles calculations based on DFT [29,30] with the screened hybrid functional of Heyd, Scuseria, and Ernzerhof (HSE) [31], as implemented in the Vienna *Ab initio* Simulation Package (VASP) [32]. The use of the hybrid functional, in which the short-range exchange potential is calculated by mixing a fraction of nonlocal Hartree-Fock exchange with the generalized gradient approximation [33], ensures a reliable description of the electronic structure, which is crucial for our present purposes. The mixing parameter (corresponding to the fraction of Hartree-Fock exchange) is set to the standard value of $\alpha = 0.25$. This choice leads to a slight underestimation of the band gap [34], but we have verified that it has a negligible impact on our calculated CB structure. We use an energy cutoff of 500 eV for the plane-wave basis set, and the core electrons are described with projector-augmented-wave potentials [35,36], with the Ba $5s^2\,5p^6\,6s^2$, Sr $4s^2\,4p^6\,5s^2$, Sn $5s^2\,5p^2$, La $5s^2\,5p^6\,6s^2\,5d^1$, and O $2s^2\,2p^4$ electrons treated as valence. An $8 \times 8 \times 8$ **k**-point grid is used for self-consistent calculations on the cubic BSO unit cell. To ensure adequate sampling of the CB, we use Wannier interpolation based on the Wannier90 code [37], with more than 200 **k**-points sampled along each high-symmetry path in the Brillouin zone. Lanthanum donors are treated in a 135-atom cubic supercell with a single special **k**-point. Spin polarization is included.

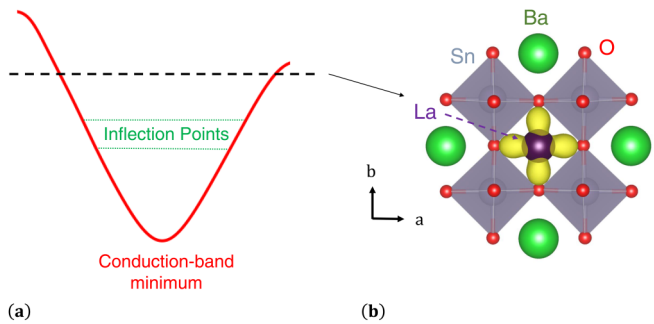

FIG. 2. (a) Schematic of the band structure of the lowest CB in BSO, showing the inflection points. The La-induced state in the CB is indicated by the dashed line. (b) Visualization of a 2D slice of the electron density associated with this state.

III. RESULTS AND DISCUSSION

A. Electronic structure

The crystal structure of BSO is a cubic, five-atom perovskite unit cell with a calculated lattice parameter of 4.13 Å. In Fig. 1, we plot the band structure, comparing results obtained directly from the HSE calculations with those obtained with Wannier interpolation. Some slight deviations are seen at higher energies, which are irrelevant for our present study. For the energy range of interest (including the inflection points) Wannier interpolation provides a close reproduction of the band shape.

The accurate energy-vs-**k** relationship that we obtain through Wannier interpolation also allows us to evaluate the band velocity and effective mass of electrons as functions of **k**. The band velocity is defined as

$$v_{\mathbf{k}} = \frac{1}{\hbar}\frac{\partial \varepsilon_{\mathbf{k}}}{\partial \mathbf{k}}, \tag{1}$$

and the effective-mass tensor is defined as

$$\left[\frac{1}{m^*_{\mathbf{k}}}\right]_{ij} = \frac{1}{\hbar^2}\frac{\partial^2 \varepsilon_{\mathbf{k}}}{\partial k_i \partial k_j}. \tag{2}$$

In Fig. 3 we plot the velocity and mass along three high-symmetry directions in the Brillouin zone, using the energy-vs-**k** relationship to show the values as a function of $\varepsilon_{\mathbf{k}}$. At the inflection point, the curvature of the conduction band goes to zero; therefore, the band velocity reaches a maximum and the effective mass diverges, changing sign once the energy is above the inflection point. These features are clearly visible in Fig. 3, as is the fact that the inflection point occurs at slightly different energies in different directions.

Based on the Wannier-interpolated band structure, we locate CB inflection points at 2.29 eV above the CBM along the $\Gamma \rightarrow$ R direction, at 2.56 eV along $\Gamma \rightarrow$ M, and at 2.31 eV along $\Gamma \rightarrow$ X. A precise identification of the inflection points

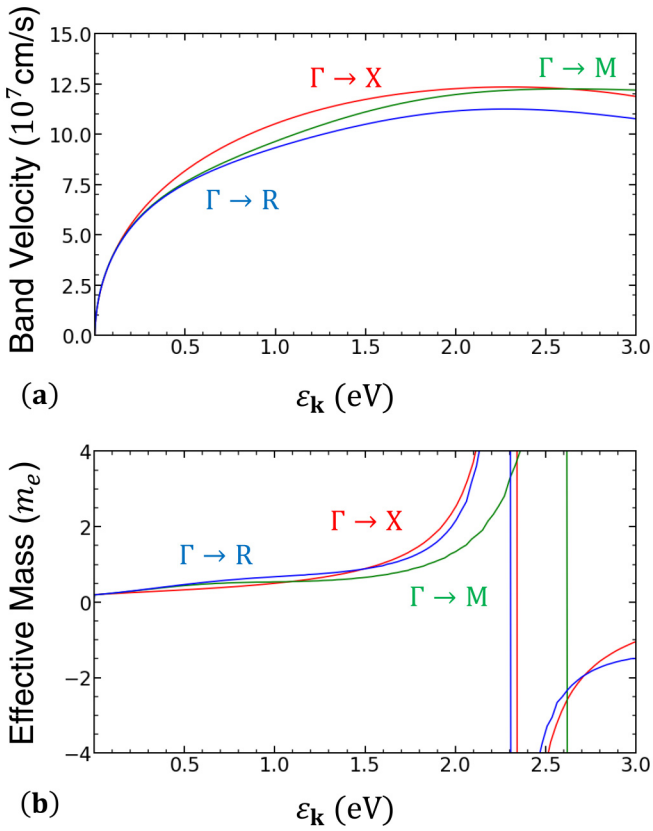

FIG. 3. (a) Band velocity and (b) effective mass of electrons for the lowest CB plotted along the Γ → X, Γ → R, and Γ → M high-symmetry directions. Values are based on Wannier-interpolated HSE results.

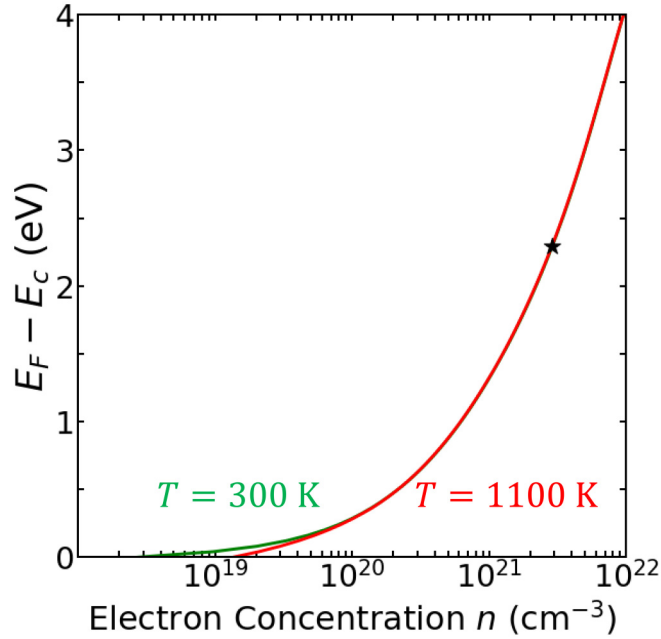

FIG. 4. The relationship between electron concentration n and Fermi level E_F, referenced to the CBM, in $BaSnO_3$ at 300 K and 1100 K, as computed from the Wannier-interpolated HSE band structure. The star indicates the position of the inflection point at 2.29 eV above the CBM.

is complicated by the fact that the CB in the vicinity of the inflection points exhibits a high degree of linearity, as indicated by the yellow highlighted parts of the band structure in Fig. 1. Specifically, the slope stays within 1% of its maximum value over ranges of 0.71 eV along Γ → X, 1.06 eV along Γ → M, and 0.61 eV along Γ → R.

Interestingly, satellite valleys occur at much higher energies than the inflection points. The lowest-energy secondary valley is located at the X point and lies 4.27 eV above the CBM, which clearly implies that intervalley scattering will not occur in BSO.

B. Conduction-band filling

Accurate knowledge of the band structure allows us to examine how E_F rises and how the CB is populated as a function of increasing electron concentration n. The relation between n and E_F can be calculated using Fermi-Dirac statistics:

$$n = \int_{E_c} \left[\exp\left(\frac{E_F - E}{k_B T}\right) + 1 \right]^{-1} g_c(E) dE \,, \qquad (3)$$

where E_c is the energy at the CBM, k_B is Boltzmann's constant, T is temperature, and $g_c(E)$ is the CB density of states (DOS). The form of $g_c(E)$ is often approximated based on a parabolic E-vs-$\mathbf{k}$ relation, but in the present case, it is essential to take the actual shape of the CB into account. Determining $g_c(E)$ numerically requires a fine mesh to accurately describe the CB energies; this required precision is enabled by Wannier interpolation. We can then numerically integrate Eq. (3) to determine n as a function of $E_F - E_c$; the results are plotted in Fig. 4. Our results are in principle more accurate than those of Ref. [17], where n vs E_F was calculated based on CB energies obtained with HSE but without the benefit of Wannier interpolation; still, the agreement is satisfactory.

To raise E_F to 2.29 eV above the CBM (the location of the Γ → R inflection point), we find that an electron concentration of 2.9×10^{21} cm^{-3} is needed. We have verified computationally that the shape of the BSO conduction band is largely unchanged, even at these high electron concentrations, such that the position of the inflection point barely varies. We note that at such high electron concentrations, the n-vs-E_F relation is approximately temperature independent, as evidenced by the negligible difference between the curves plotted in Fig. 4. To be specific, the electron concentration at $E_F - E_c = 2.29$ eV changes by less than 1% between 300 K and 1100 K. The concentration of 2.9×10^{21} cm^{-3} is less than 50% larger than the maximum concentration obtained experimentally to date [15]. However, it is not implausible that experimental concentrations can be raised by further optimizing synthesis and doping conditions.

C. Limits of La doping

We now assess whether the La-induced level in the CB is high enough to enable doping up to E_F values approaching the inflection point. For this purpose, we perform a calculation of La_{Ba} in a supercell and examine the nature of the wave functions for unoccupied states. The host-related states with energies above the CBM are delocalized, as is characteristic

of extended CB states. At an energy 4.32 eV above the CBM, we find a state that is localized on the La impurity; this state is depicted in Fig. 2(b), with lobes extending into and out of the page removed for clarity. Inspection of the localized state indicates that it has primarily La-5*d* character; 4*f*-related states occur at higher energies. We can conclude that localization of the electron on the La donor would set in only at 4.32 eV above the CBM, indicating that La will behave as an electron donor up to that point.

We have not attempted to address the effect of La concentration. The finite concentration of La in our supercell leads to dispersion of the state that is localized on the impurity, reflecting the formation of an impurity band. The value reported above, extracted using the special-point formalism, should be representative of the dilute limit. The dispersion of the impurity band may differ with the La concentration; however, the La level still remains well above the inflection point at 2.29 eV.

The first-principles calculations of Refs. [27] and [28] indicated that doping with La_{Ba} can lead to electron concentrations exceeding 10^{21} cm^{-3}, particularly under Ba-poor and O-poor conditions. It is important to note that in those assessments it was assumed that the solubility of La_{Ba} was limited by equilibrium with a La_2O_3 phase. It has been proposed [38] that such limits can be overcome under certain regimes, raising the prospect for doping beyond this "solubility limit." More concerning is the potential formation of compensating defects. References [27,28] concluded that compensating species did not form, but neither considered La concentrations beyond the limit imposed by La_2O_3 formation. Cation vacancies (V_{Ba} and V_{Sn}) are the biggest concern, and means to suppress their formation would need to be devised.

D. Band-structure engineering via alloying

Finally, we consider the possibility of alloying BSO with another ABO_3 perovskite in which the inflection point lies at a lower energy with respect to the CBM, thus making it easier to reach (by either electron injection or doping). Our survey of potential candidates indicates that the materials in which the inflection point lies lower also tend to have a CBM that occurs at a higher energy, thus rendering electron injection or high doping more difficult. Alloying will thus involve a tradeoff.

Staying within the stannates, $SrSnO_3$ (SSO) may appear to be an obvious candidate on account of its chemical similarity; however, our analysis of its band structure reveals an absence of inflection points. We attribute this observation to the lower symmetry of SSO. While BSO is cubic, SSO is orthorhombic with a 20-atom unit cell. The larger real-space unit cell leads to a smaller Brillouin zone, and the resulting band folding (combined with effects of atomic displacements within the cell) removes the inflection points from the band structure.

Next, we consider alloying candidates with different elements on the B site. $BaZrO_3$ (BZO) is a cubic perovskite oxide with a calculated lattice parameter of 4.20 Å, quite similar to BSO (4.13 Å). The band gap of BZO is indirect with a value of 4.52 eV, with the VBM at R and the CBM at Γ, just like in BSO. We find that BZO has an inflection point in its lowest CB that appears at just 0.23 eV above the CBM in the Γ → X direction (indicative of low dispersion along this direction). The secondary CB valleys are also lower in energy than in BSO, with the X valley lying only 0.43 eV above the CBM. These features indicate that BZO would not be of interest for achieving NDR itself, but alloying BZO with BSO might help to bring the inflection point closer to the CBM. Solid solutions of BSO and BZO have not been widely investigated to date; one study reported alloys of $Ba(Sn_{1-x}Zr_x)O_3$ (BSZO) up to 10 mol% Zr [39].

IV. CONCLUSIONS

In summary, we have performed a comprehensive examination of the CB structure of BSO and the consequences for electron doping and transport. We identified an inflection point 2.29 eV above the CBM along Γ → R. Satellite valleys all occur at much higher energies. Accurate calculations of the DOS indicate that to raise E_F to the inflection point, an electron concentration of 2.9×10^{21} cm^{-3} is needed. We have verified that La remains an electron donor up to the inflection point. Appropriate control of growth conditions and dopant incorporation should make higher Fermi levels accessible through doping, potentially enabling devices based on NDR.

ACKNOWLEDGMENTS

We thank S. Stemmer and D. Jena for useful discussions. This work was supported by the Office of Naval Research (ONR) under Grant No. N00014-18-1-2704. A.J.E.R. was also supported by the National Science Foundation (NSF) Graduate Research Fellowship Program under Grant No. 1650114. Any opinions, findings, and conclusions or recommendations expressed in this material are those of the author(s) and do not necessarily reflect the views of the NSF. We acknowledge computational resources provided by the Extreme Science and Engineering Discovery Environment (XSEDE), which is supported by NSF Grant No. ACI-1548562. Use was also made of computational facilities purchased with funds from NSF (CNS-1725797) and administered by the Center for Scientific Computing (CSC). The CSC is supported by the California NanoSystems Institute and the Materials Research Science and Engineering Center (NSF DMR-1720256) at UC Santa Barbara.

[1] Z. Xia, C. Wang, N. K. Kalarickal, S. Stemmer, and S. Rajan, IEEE Trans. Electron Dev. **66**, 896 (2019).

[2] H. J. Kim, U. Kim, H. M. Kim, T. H. Kim, H. S. Mun, B.-G. Jeon, K. T. Hong, W.-J. Lee, C. Ju, K. H. Kim, and K. Char, Appl. Phys. Express. **5**, 061102 (2012).

[3] S. Ismail-Beigi, F. J. Walker, S. W. Cheong, K. M. Rabe, and C. H. Ahn, APL Mater. **3**, 062510 (2015).

[4] H. Paik, Z. Chen, E. Lochocki, A. Seidner, A. Verma, N. Tanen, J. Park, M. Uchida, S. Shang, B.-C. Zhou, M. Brützam, R. Uecker, Z.-K. Liu, D. Jena, K. M. Shen,

D. A. Muller, and D. G. Schlom, APL Mater. **5**, 116107 (2017).
[5] P. Singh, A. Swartz, D. Lu, S. S. Hong, K. Lee, A. F. Marshall, K. Nishio, Y. Hikita, and H. Y. Hwang, ACS Appl. Electron. Mater. **1**, 1269 (2019).
[6] S. J. Allen, S. Raghavan, T. Schumann, K.-M. Law, and S. Stemmer, Appl. Phys. Lett. **108**, 252107 (2016).
[7] K. Krishnaswamy, B. Himmetoglu, Y. Kang, A. Janotti, and C. G. Van de Walle, Phys. Rev. B **95**, 205202 (2017).
[8] H. Mizoguchi, H. W. Eng, and P. M. Woodward, Inorg. Chem. **43**, 1667 (2004).
[9] H. Krömer, Phys. Rev. **109**, 1856 (1958).
[10] H. Kroemer, in *Progress in Semiconductors*, edited by A. F. Gibson (John Wiley, New York, 1960), Vol. IV, p. 1.
[11] Q. Yan, E. Kioupakis, D. Jena, and C. G. Van de Walle, Phys. Rev. B **90**, 121201(R) (2014).
[12] J. Gunn, Solid State Commun. **1**, 88 (1963).
[13] H. Kroemer, Proc. IEEE **52**, 1736 (1964).
[14] Z. S. Gribnikov, R. R. Bashirov, and V. V. Mitin, IEEE J. Sel. Top. Quantum Electron. **7**, 630 (2001).
[15] H. F. Wang, Q. Z. Liu, F. Chen, G. Y. Gao, and W. Wu, J. Appl. Phys. **101**, 106105 (2007).
[16] A. Janotti, L. Bjaalie, L. Gordon, and C. G. Van de Walle, Phys. Rev. B **86**, 241108(R) (2012).
[17] K. Krishnaswamy, L. Bjaalie, B. Himmetoglu, A. Janotti, L. Gordon, and C. G. Van de Walle, Appl. Phys. Lett. **108**, 083501 (2016).
[18] K. Fujiwara, K. Nishihara, J. Shiogai, and A. Tsukazaki, AIP Adv. **6**, 085014 (2016).
[19] A. Prakash, N. F. Quackenbush, H. Yun, J. Held, T. Wang, T. Truttmann, J. M. Ablett, C. Weiland, T.-L. Lee, J. C. Woicik, K. A. Mkhoyan, and B. Jalan, Nano Lett. **19**, 8920 (2019).
[20] T. R. Paudel and E. Y. Tsymbal, Phys. Rev. B **96**, 245423 (2017).
[21] Y. Kim, Y. M. Kim, J. Shin, and K. Char, APL Mater. **6**, 096104 (2018).
[22] L. Bjaalie, B. Himmetoglu, L. Weston, A. Janotti, and C. G. Van de Walle, New J. Phys. **16**, 025005 (2014).
[23] S. A. Chambers, T. C. Kaspar, A. Prakash, G. Haugstad, and B. Jalan, Appl. Phys. Lett. **108**, 152104 (2016).
[24] S. Raghavan, T. Schumann, H. Kim, J. Y. Zhang, T. A. Cain, and S. Stemmer, APL Mater. **4**, 016106 (2016).
[25] A. Prakash, P. Xu, A. Faghaninia, S. Shukla, J. W. Ager III, C. S. Lo, and B. Jalan, Nat. Commun. **8**, 15167 (2017).
[26] D. O. Scanlon, Phys. Rev. B **87**, 161201(R) (2013).
[27] L. Weston, L. Bjaalie, K. Krishnaswamy, and C. G. Van de Walle, Phys. Rev. B **97**, 054112 (2018).
[28] S. KC, A. J. E. Rowberg, L. Weston, and C. G. Van de Walle, J. Appl. Phys. **126**, 195701 (2019).
[29] P. Hohenberg and W. Kohn, Phys. Rev. **136**, B864 (1964).
[30] W. Kohn and L. J. Sham, Phys. Rev. **140**, A1133 (1965).
[31] J. Heyd, G. E. Scuseria, and M. Ernzerhof, J. Chem. Phys. **118**, 8207 (2003).
[32] G. Kresse and J. Furthmüller, Phys. Rev. B **54**, 11169 (1996).
[33] J. P. Perdew, K. Burke, and M. Ernzerhof, Phys. Rev. Lett. **77**, 3865 (1996).
[34] Y. Kang, H. Peelaers, K. Krishnaswamy, and C. G. Van de Walle, Appl. Phys. Lett. **112**, 062106 (2018).
[35] P. E. Blöchl, Phys. Rev. B **50**, 17953 (1994).
[36] G. Kresse and D. Joubert, Phys. Rev. B **59**, 1758 (1999).
[37] G. Pizzi, V. Vitale, R. Arita, S. Blügel, F. Freimuth, G. Géranton, M. Gibertini, D. Gresch, C. Johnson, T. Koretsune, J. Ibañez-Azpiroz, H. Lee, J.-M. Lihm, D. Marchand, A. Marrazzo, Y. Mokrousov, J. I. Mustafa, Y. Nohara, Y. Nomura, L. Paulatto, S. Poncé, T. Ponweiser, J. Qiao, F. Thöle, S. S. Tsirkin, M. Wierzbowska, N. Marzari, D. Vanderbilt, I. Souza, A. A. Mostofi, and J. R. Yates, J. Phys.: Condens. Matter **32**, 165902 (2020).
[38] S. Zhang, J. Phys.: Condens. Matter **14**, R881 (2002).
[39] V. Jayaraman, G. Mangamma, T. Gnanasekaran, and G. Periaswami, Solid State Ionics **86**, 1111 (1996).